doi:10.1093/brain/awaa089 BRAIN 2020: 143; 1341–1349 | 1341

BRAIN
A JOURNAL OF NEUROLOGY

REPORT

Relationship between cortical iron and tau aggregation in Alzheimer's disease

Nicola Spotorno,[1,2] Julio Acosta-Cabronero,[3] Erik Stomrud,[2,4] Björn Lampinen,[5] Olof T. Strandberg,[2] Danielle van Westen[2,6] and Oskar Hansson[2,4]

A growing body of evidence suggests that the dysregulation of neuronal iron may play a critical role in Alzheimer's disease. Recent MRI studies have established a relationship between iron accumulation and amyloid-β aggregation. The present study provides further insight demonstrating a relationship between iron and tau accumulation using magnetic resonance-based quantitative susceptibility mapping and tau-PET in $n = 236$ subjects with amyloid-β pathology (from the Swedish BioFINDER-2 study). Both voxel-wise and regional analyses showed a consistent association between differences in bulk magnetic susceptibility, which can be primarily ascribed to an increase in iron content, and tau-PET signal in regions known to be affected in Alzheimer's disease. Subsequent analyses revealed that quantitative susceptibility specifically mediates the relationship between tau-PET and cortical atrophy measures, thus suggesting a modulatory effect of iron burden on the disease process. We also found evidence suggesting the relationship between quantitative susceptibility and tau-PET is stronger in younger participants (age $\leqslant 65$). Together, these results provide *in vivo* evidence of an association between iron deposition and both tau aggregation and neurodegeneration, which help advance our understanding of the role of iron dysregulation in the Alzheimer's disease aetiology.

1 Penn Frontotemporal Degeneration Center, Department of Neurology, University of Pennsylvania Perelman School of Medicine, Philadelphia, PA, USA
2 Clinical Memory Research Unit, Department of Clinical Sciences, Malmö, Lund University, Lund, Sweden
3 Tenoke Ltd., Cambridge, UK
4 Memory Clinic, Skåne University Hospital, Malmö, Sweden
5 Clinical Sciences Lund, Medical Radiation Physics, Lund University, Lund, Sweden
6 Diagnostic Radiology, Department of Clinical Sciences, Lund University, Lund, Sweden

Correspondence to: Oskar Hansson
Memory Clinic,
Skåne University Hospital, Malmö, Sweden
E-mail: oskar.hansson@med.lu.se

Keywords: iron; tau; quantitative susceptibility mapping; Alzheimer's disease; tau-PET

Abbreviations: ITG = inferior temporal gyrus; QSM = quantitative susceptibility mapping

Introduction

Past *in vitro* and post-mortem studies have suggested there is a relationship between excessive iron deposition and the hallmarks of Alzheimer's disease proteinopathy, namely amyloid-β plaques and neurofibrillary tangles (Sayre *et al.*, 2000; Everett *et al.*, 2014). Neuronal iron is likely to be the major source of contrast captured by MRI using a technique called quantitative susceptibility mapping (QSM), which quantifies magnetic susceptibility, a fundamental electromagnetic property (Langkammer *et al.*, 2012).

Recent neuroimaging studies have linked iron accumulation, as measured by QSM, with both fibrillar amyloid

Received September 2, 2019. Revised February 5, 2020. Accepted February 10, 2020. Advance access publication April 24, 2020

accumulation and rate of cognitive decline (Acosta-Cabronero *et al.*, 2013; van Bergen *et al.*, 2016; Ayton *et al.*, 2017; Kim *et al.*, 2017). However, *in vivo* studies investigating a possible relationship between iron accumulation and pathological tau aggregation are still lacking.

Considering neuronal iron accumulation has been associated with both normal ageing (Ward *et al.*, 2014) and neurodegenerative processes (Pérez *et al.*, 1998; Ayton and Lei, 2014; Bulk *et al.*, 2018*a*), it follows that understanding the interaction between abnormal iron homeostasis and abnormal tau aggregation in Alzheimer's disease could provide new insights into Alzheimer's disease pathogenesis and lead to new therapeutic targets.

Recently, Ayton *et al.* (2019) carried out an *ex vivo* study suggesting an association between iron accumulation in the inferior temporal gyrus (ITG) and steeper rate of cognitive decline in subjects showing significant amyloid-β plaques and tau tangles. The authors found that the sites of increased iron content were non-overlapping with amyloid plaque formation, but that sites of increased iron content were spatially co-localized with areas of tau burden. An association between iron, as measured by an iron-sensitive MRI sequence (T_2*), and tau accumulation was also found in a combined post-mortem MRI and histological study from Bulk *et al.* (2018*b*). However, another *ex vivo* study that used T_2* along with immunohistochemistry found no conclusive evidence of association between iron accumulation and tau accumulation when taking a pixel-based spatial correlation approach (Bulk *et al.*, 2018*a*).

In the present prospective *in vivo* study, we used state-of-the-art imaging techniques (QSM and tau-PET) to examine the potential relationship between measures of iron accumulation and abnormal tau aggregation in the Alzheimer's disease continuum, which is characterized by evidence of cerebral amyloidosis according to the recent NIA-AA research framework (Jack *et al.*, 2018). We explored the association between QSM and tau-PET both at the voxel-grey matter level and in a region of interest analysis focusing on the ITG, a region known to be severely affected by tau pathology in Alzheimer's disease and commonly assessed with tau-PET (Vogel *et al.*, 2019). We also investigated the possible mediation effect of iron content (as measured with QSM) on the link between tau aggregation and neuronal loss, the latter approximated by cortical thickness measurements from structural MRI.

Materials and methods

Participants

Two hundred and thirty-six participants from the Swedish BioFINDER-2 study were included (see Supplementary material for inclusion and exclusion criteria). Only participants with CSF biomarker evidence of cerebral amyloidosis (abnormal amyloid-$\beta_{42/40}$ ratio) were included in the study cohort, which consisted of 78 cognitively unimpaired amyloid-β-positive subjects and 158 cognitively impaired patients. The latter group consisted of 77 amyloid-β-positive patients diagnosed with mild cognitive impairment and 81 patients with Alzheimer's disease dementia. Demographic and clinical characteristics of the participants are summarized in Table 1. All subjects gave written informed consent according to the Declaration of Helsinki, and the study was approved by the Ethical Review Board of Lund, Sweden.

Table 1 Demographic summary of the study cohort

	Cognitively unimpaired	Cognitively impaired
n (female)	78 (38)	158 (86)
Age	73 (8)	73 (6)
Years of education	12 (4)	12 (4)[a]
MMSE	29 (1)	23 (5)*
Cortical QSM	0.001 (0.001)	0.002 (0.002)
Cortical tau-SUVR	1.08 (0.13)	1.40 (0.41)*
ITG QSM	0.0003 (0.0019)	0.0010 (0.0020)*
ITG tau-SUVR	1.26 (0.21)	1.95 (0.82)*

Values are given as mean (standard deviation). Demographic factors and clinical characteristics were compared using χ^2 and Mann-Whitney U-tests (Sex: $\chi^2 = 0.47$, $P > 0.4$; age: U = 5934, $P > 0.3$; years of education: U = 6062, $P > 0.4$; MMSE: U = 881, $P < 0.001$; cortical QSM: U = 5515, $P = 0.095$; cortical tau-SUVR: U = 2396, $P < 0.001$; ITG QSM: U = 4628, $P < 0.01$; ITG tau-SUVR: U = 2181, $P < 0.001$).
*Significantly different from the cognitively unimpaired group. MMSE = Mini-Mental State Examination.
[a]Three datapoints were missing.

Imaging protocol

MRI protocol

MRI data were acquired on a Siemens Prisma 3 T scanner with a 64-channel receiver-coil array (Siemens Healthcare). Susceptibility weighting was sensitized with a 3D, multi gradient-echo pulse sequence: the first echo was flow-compensated; flip angle = 15°; echo times = 5.00, 8.80, 12.60, 16.40 and 20.20 ms (monopolar/fly-back readout gradients); receiver bandwidth = 490 Hz/pixel; repetition time = 24 ms; voxel size = 0.8 × 0.8 × 1.4 mm^3; 6/8 partial Fourier; scan time = 3:54 min. MPRAGE (magnetization-prepared, 3D, rapid gradient-echo) anatomical images were also acquired with the following acquisition parameters: inversion time = 1100 ms; flip angle = 9°; echo time = 2.54 ms; echo spacing = 7.3 ms; repetition time = 1900 ms; receiver bandwidth = 220 Hz/pixel, and voxel size = 1 × 1 × 1 mm^3, scan time = 5:15 min. GRAPPA (generalized autocalibrating partially parallel acquisitions; Griswold *et al.*, 2002) was applied with acceleration factor of 2 and 24 reference lines in both sequences.

PET protocol

The second-generation tau-PET tracer ^{18}F-RO-948 (previously known as ^{18}F-RO6958948) was synthesized at Skåne University Hospital, Lund, and PET scans were performed on a GE Discovery 690 PET scanner (General Electric Medical Systems). FreeSurfer parcellation (v6; http://surfer.nmr.mgh.harvard.edu/), carried out in anatomical MRI space, was applied to processed, co-registered, and time-averaged PET images in order to extract regional uptake values. ^{18}F-RO-948 standardized uptake value ratio (SUVR) images were obtained from the mean uptake over a 70–90 min post-injection interval (Kuwabara *et al.*, 2018), globally normalized to the mean uptake in an inferior cerebellar grey matter (reference) region (Maass *et al.*, 2017).

CSF protocol and analysis

Lumbar CSF sampling was performed according to the Alzheimer's Association Flow Chart (Blennow *et al.*, 2010). Samples were stored in 1 ml polypropylene tubes at −80°C until analysis. ELISA was used for analysis of CSF amyloid-β_{40} and amyloid-β_{42} (Mesoscale Discovery). Amyloid-β-positivity was defined as CSF amyloid-$\beta_{42/40} \leqslant 0.89$ according to clinical routine practice. All analyses were performed by board certified laboratory technicians who were blinded to clinical diagnoses.

MRI reconstruction and post-processing

QSM reconstruction

Multi-channel complex data were combined using the adaptive combination method implemented on Siemens firmware version E11C. Subsequent processing steps were performed with the combined multi-echo pipeline (see the Supplementary material for modifications) in QSMbox (https://gitlab.com/acostaj/QSMbox), including the multi-scale dipole inversion (MSDI) algorithm described elsewhere (Acosta-Cabronero *et al.*, 2018; Supplementary material and Supplementary Figs 1 and 2).

QSM post-processing

QSM reconstructed data were post-processed and analysed using QSMexplorer routines (https://gitlab.com/acostaj/QSMexplorer). In short, a study-specific template was created for the BioFINDER-2 cohort using radio-frequency bias corrected MPRAGE images from 125 pseudo-randomly selected participants including both healthy controls and neurodegenerative disease patients. QSM spatial standardization was achieved with a previously optimized method, which uses a combination of ANTs v2.1 (http://stnava.github.io/ANTs), SPM12 (http://www.fil.ion.ucl.ac.uk/spm/software/spm12) and FSL-v5.10 (FMRIB Software Library) tools (Acosta-Cabronero *et al.*, 2016*a*) (Supplementary material). To avoid making assumptions about areas being spared in patients, the main QSM results are shown with zero-centred data (as in Acosta-Cabronero *et al.*, 2017, 2018*a*). Results with QSM values referenced to a deep prefrontal white matter region are also included in Supplementary Fig. 3.

Statistical analysis

The relationships between demographic variables and clinical status (i.e. diagnosis) were evaluated with chi-square and Mann-Whitney U-tests implemented in Python 3.6 (Table 1).

Voxel-wise grey matter QSM cluster-enhanced analysis

Absolute susceptibility maps were used for whole-brain analysis to prevent convolution-driven cancellations of spatially adjacent positive/negative susceptibilities (Betts *et al.*, 2016); these were smoothed using a Gaussian kernel with a standard deviation of 3 mm and additional compensation for brain-boundary effects. As some QSM variance will result from age differences (Acosta-Cabronero *et al.*, 2016), age was introduced as a nuisance covariate in our statistical model. The QSM maps were downsampled to a 2 mm^3 resolution to minimize the computational processing load. However, a supplementary analysis with 1 mm^3 for a randomly selected group of 191 participants was been performed (Supplementary Fig. 4). For tau-PET, we focused on a region of interest most typically associated with tau aggregation in Alzheimer's disease, i.e. a temporal meta-region of interest reflecting Braak stages I–IV (Cho *et al.*, 2016; Jack *et al.*, 2017) and spanning bilateral entorhinal, fusiform, inferior and middle temporal cortices. The mean SUVR values extracted from this region of interest for all subjects were introduced as a covariate of interest in our study design. The voxel-wise regression analysis was restricted to a grey matter mask based on SPM12 tissue segmentation and was performed with threshold-free, cluster-enhanced permutation statistics using FSL *randomise* (http://fsl.fmrib.ox.ac.uk/fsl/fslwiki/Randomise) with 10 000 permutations. Whole-brain statistical significance was set at the stringent family-wise error corrected threshold of $P < 0.01$.

Regional analysis

To establish the directionality of QSM differences, and to investigate local associations between QSM and tau-PET, mean regional SUVR and signed QSM values were extracted from the 68 bilateral cortical regions of the Desikan-Killiany-Tourville atlas included in FreeSurfer v6. Mean regional cortical thickness was also calculated (Supplementary material). The Pearson product-moment correlation coefficient in each region was computed and statistical significance was established at the false discovery rate (FDR) corrected threshold, $P < 0.05$. More detailed regional analyses were performed for the ITG, namely, multiple regression analyses testing for an association between mean regional QSM and both mean tau-PET SUVR and mean cortical thickness including the cognitive status (cognitively unimpaired and cognitively impaired participants) into the regression model. The cohort was further subdivided into younger and older groups based on a cut-off of 65 years of age, which is the upper limit for early onset Alzheimer's dementia as well as a widely recognized threshold of old age (Rossor *et al.*, 2010). A mediation analysis to test the effect of QSM on the association between tau-PET tracer uptake and cortical thickness was performed and the statistical significance of the mediation effect was tested with bootstrapping (10 000 samples) (Hayes, 2009; see also the Supplementary material). Models included cognitive status as covariate as well as age and sex. Analyses were performed in Python 3.6. and RStudio v1.1.463 (see Supplementary material for a further analysis in which the cohorts have been divided in cognitively impaired participants and cognitively unimpaired participants.)

Data availability

Anonymized data will be shared by request from a qualified academic investigator for the sole purpose of replicating procedures and results presented in the article and as long as data transfer is in agreement with EU legislation on the general data protection regulation and decisions by the Ethical Review Board of Sweden and Region Skåne.

Results

Whole grey matter QSM analysis

The voxel-wise regression analysis revealed that tau-PET uptake in temporal lobe regions (temporal meta-region of interest) is primarily associated with widespread absolute susceptibility increases in temporal regions encompassing bilateral inferior and middle temporal gyrus, fusiform gyrus,

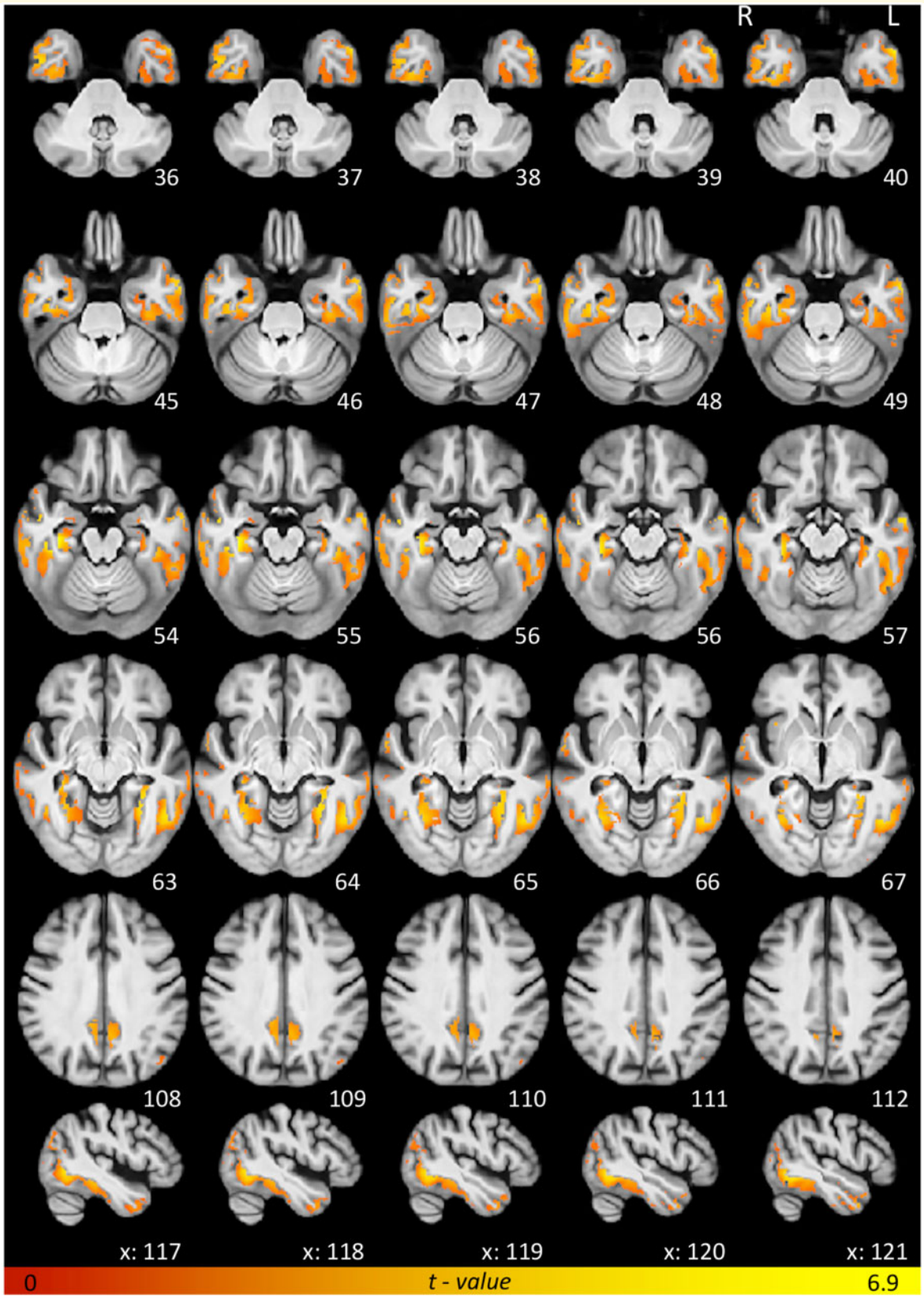

Figure 1 Whole grey matter QSM voxel-wise regression results. Clusters display the *t*-values for the significant results ($P < 0.01$ FWE) of the positive voxel-wise association: absolute-QSM ~ tau-SUVR + age. The results are displayed in radiological convention. For visualization purposes the results have been warped to MNI space (Montreal Neurological Institute template) 152 using ANTs routines and displayed over the study-wise anatomical template.

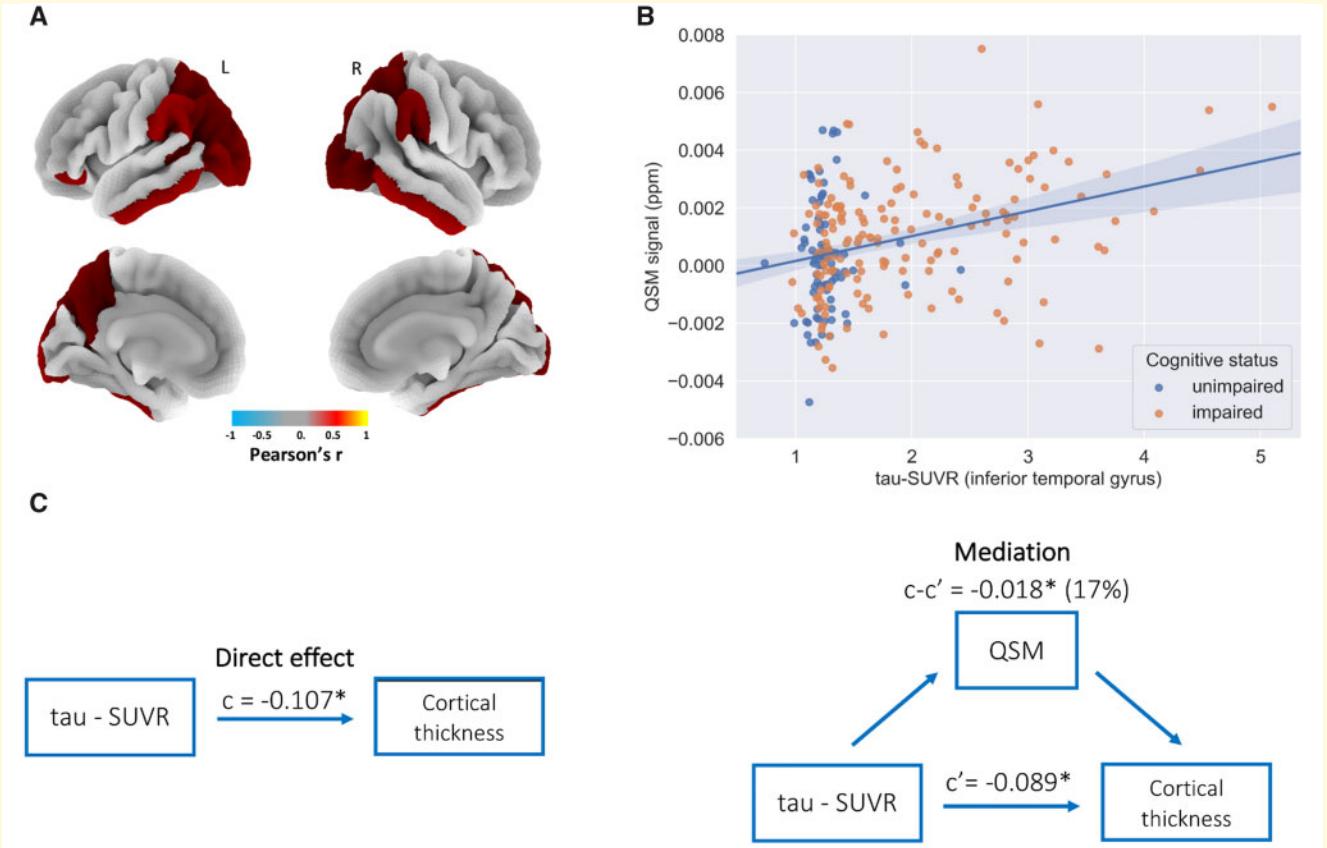

Figure 2 Regional analysis for the full study cohort. (**A**) Regional pattern of significant Pearson Product-Moment correlation (FDR corrected $P < 0.05$) between signed-QSM and tau-PET signal. The colour scale represents the Pearson correlation coefficient. (**B**) Signed-QSM plotted as a function of mean normalized tau-PET tracer uptake in the inferior temporal gyrus. The translucent area around the regression line represents the 95% CI for the regression estimate. (**C**) Flow chart illustration of the mediation analysis results (each model includes age sex and cognitive group as covariates); c represents the direct association strength between tau-PET signal and cortical thickness [$\beta = -0.107$, $P < 0.0001$, CI: –0.13 to –0.08]; c' is the association strength between tau-PET signal and cortical thickness accounting for the effect of QSM [$\beta = -0.089$, $P < 0.001$, CI: –0.12 to –0.06]; c-c' is therefore the mediation effect of QSM [$\beta = -0.018$, $P < 0.001$, CI: –0.03 to –0.01, QSM can explain 17% (β_{ratio}) of the effect of tau-PET signal on cortical thickness].

parahippocampal cortex and temporal pole. In addition, although more sparse, QSM in parietal areas (especially the supramarginal gyrus), precuneus, posterior cingulate cortex, lateral occipital and frontal areas such as the middle frontal cortex and insular cortex also covaried with temporal lobe tau-PET tracer uptake (Fig. 1 and Supplementary Table 1). The reverse contrast, i.e. negative correlations between absolute QSM and tau-PET values, was not significant across the whole brain.

Regional analysis

The regional pattern of statistically significant correlation between signed QSM and tau-PET values is shown as a 3D overlay in Fig. 2A (and further summarized in Supplementary Table 2; see also Supplementary Figs 5 and 6A). The regional analyses confirmed that the positive absolute QSM correlations identified by the whole-brain analysis are indeed driven by local increases in signed QSM, which is consistent with a scenario of iron accumulation. The ITG returned the strongest regional QSM/tau-PET correlation [left ITG: $r = 0.31$, $P < 0.001$ FDR; right ITG: $r = 0.32$, $P < 0.001$ FDR].

Further analysis in the ITG (averaged across hemispheres, and accounting for possible confounding effects of age and sex and including cognitive status as a covariate) confirmed a positive association between susceptibility-MRI and tau-PET measures (Fig. 2B) [tau-PET: $\beta = 0.0009$, $P < 0.001$, confidence interval (CI) = 0.001 to 0.001; cognitively unimpaired and cognitively impaired (Cog) group : $\beta = -0.0002$, $P > 0.5$, CI = –0.001 to 0, age: $\beta = 5.8 \times 10^{-5}$, $P = 0.001$, CI = 2.5×10^{-5} to 9.1×10^{-5}; sex: $\beta = 0.0001$, $P > 0.6$, CI = 0 to 0.001]. Of note, the correlation between QSM in the ITG and age was significant. In addition, both tau-PET and QSM values in the ITG were negatively associated with cortical thickness measures (Supplementary material). The mediation analysis revealed that the association between tau-PET and cortical thickness was partially mediated by QSM also when including the cognitive status in the model [mediation effect = 17%; $\beta = -0.018$, $P < 0.001$, CI: –0.03

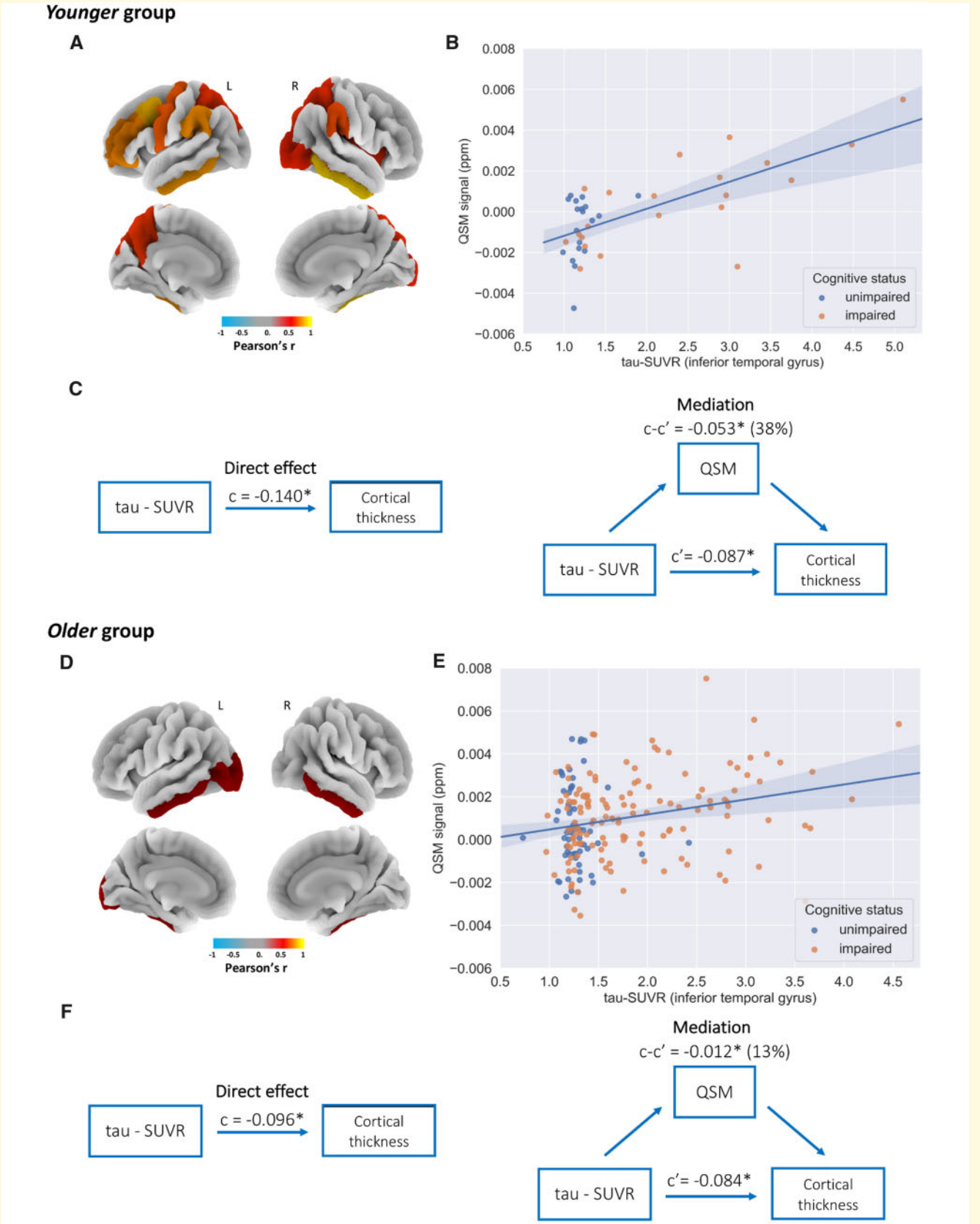

Figure 3 Regional analyses for younger and older groups. (**A**–**C**) Results for the younger group (n = 40). (**A**) Regional pattern of significant Pearson's correlation between signed-QSM and tau-PET signal (FDR corrected $P < 0.05$). The colour scale represents the Pearson correlation coefficient. (**B**) Covariation of signed-QSM with respect to tau-PET values extracted from the inferior temporal gyrus. The translucent area around the regression line represents the 95% CI for the regression estimate. (**C**) Flow chart representing the mediation analysis (each

(continued)

to –0.01] (Fig. 2C). A regression model including age, sex and education level (in years) as nuisance covariate showed a significant negative correlation between QSM signal in the ITG and global cognition as quantified by the Mini-Mental State Examination (MMSE) [QSM: $\beta = -739$, $P < 0.001$, CI: –1067 to –410; age: $\beta = 0.039$, $P > 0.3$, CI: –0.050 to 0.128; sex: $\beta = -0.63$, $P > 0.3$, CI: –1.87 to 0.60; education: $\beta = 0.12$, $P > 0.1$, CI: –0.03 to 0.27] (Supplementary Figs 7 and 8).

The age-split revealed that the association between QSM and tau-PET is more pronounced in younger amyloid-β-positive individuals ($\leqslant$65 years old, $n = 40$) (Fig. 3A, B, D and E, Supplementary Tables 3 and 4, and Supplementary Fig. 6D and E) [(regression model in the ITG): adjust-R^2 = 0.48; tau-PET: $\beta = 0.0015$, $P < 0.001$, CI = 0.001 to 0.002; Cog group: $\beta = 0.0002$, $P > 0.7$, CI = –0.001 to 0.001; age: $\beta = -0.0002$, $P = 0.09$, CI = 0 to 2.7×10^{-5}; sex: $\beta = -0.0005$, $P > 0.3$, CI = –0.001 to 0.001] than in those who are older [$n = 196$ (regression model in the ITG): adjust-R^2 = 0.06; tau-PET: $\beta = 0.0007$, $P < 0.005$, CI = 0 to 0.001; Cog group: $\beta = 0.0002$, $P > 0.5$, CI = –0.001 to 0; age: $\beta = 3.8 \times 10^{-5}$, $P > 0.1$, CI = -1.3×10^{-5} to 8.9×10^{-5}; sex: $\beta = 0.0002$, $P < 0.2$, CI = 0 to 0.001]. The mediation effect by QSM on the association between tau-PET and cortical thickness was also stronger in the younger group (mediation effect = 38% versus 13% for the older group) (Fig. 3C and F) also when accounting for the different cognitive statuses of the participants (see Supplementary material, Supplementary Tables 3–7 and Supplementary Figs 6 and 9–11 for the results of the analyses stratified by cognitive status).

Discussion

This study explored the relationship between iron content (cortical QSM) and tau burden (tau-PET tracer) in Alzheimer's disease. The whole grey matter QSM regression analysis revealed a pattern of magnetic susceptibility correlations with tau-PET uptake in a temporal meta-region of interest that is consistent with the spatial distribution of tau deposition in Alzheimer's disease (Braak and Braak, 1991; Vogel *et al.*, 2019). The subsequent regional analyses further supported an association between increased (signed) QSM values—reflective of increased iron content—and tau accumulation, which was strongest in the ITG. Furthermore, we found a significant mediation effect of QSM on the relationship between tau-PET and cortical thickness. Finally, an age split revealed that both the association between QSM and tau-PET and the mediation effect of QSM was stronger in younger than in older participants.

Although the cross-sectional nature of our study design renders us unable to speculate whether abnormal iron homeostasis precedes, or follows, proteinopathy in Alzheimer's disease, the present results support the hypothesis that iron accumulation is a co-factor involved in neurodegeneration in Alzheimer's disease.

The interaction between tau misfolding, iron accumulation and neurodegeneration is likely quite complex. One possible interpretation of our results is that tau dysfunction and misfolding could result in iron deposition, ultimately leading to oxidative stress and neuronal loss or ferroptosis (Dixon *et al.*, 2012). It is also plausible that iron dysregulation could generate a toxic environment that could contribute to tau misfolding and other neurotoxic events. This theory is consistent with past *in vitro* studies that have shown that iron can induce both tau phosphorylation (Lovell *et al.*, 2004) and tau aggregation (Yamamoto *et al.*, 2002). The current data and previous findings (Lei *et al.*, 2012) support the concept that at least part of the toxicity occurs through soluble tau-dependent, iron-induced oxidative damage or ferroptosis. Our results suggested also that iron accumulation is related with cognitive decline. QSM signal in the ITG was, indeed, associated with the level of cognitive impairment as measured by MMSE. The association between QSM signal in the ITG and MMSE recapitulates *in vivo* the association between the *ex vivo* quantification of iron accumulation in the ITG and MMSE recently presented by Ayton *et al.* (2019). However, longitudinal studies will be necessary to clarify the nature of the interaction between iron, tau and degeneration in different stages of the disease process.

Past studies have also shown higher levels of neuronal iron, as well as differences in iron-sensitive MRI metrics, in early-onset with respect to late-onset disease (Bulk *et al.*, 2018*b*). Here, we found differential iron-related results between younger and older groups but as our younger group was small in size and statistically underpowered, further

Figure 3 Continued

model includes age sex and cognitive group as covariates). c = direct association between tau-PET signal and cortical thickness [$\beta = -0.14$, $P < 0.001$, CI: –0.20 to –0.10]; c' = association between tau-PET signal and cortical thickness accounting for the effect of QSM [$\beta = -0.087$, $P < 0.005$, CI: –0.145 to –0.03]; c-c' = mediation effect of QSM [$\beta = -0.053$, $P < 0.005$, CI: –0.104 to –0.02, QSM explains 38% (β_{ratio}) of the effect of tau-PET signal on cortical thickness]. (**D**–**F**) Results for the older group ($n = 196$). (**D**) Regions in which the Pearson Product-Moment correlation between signed-QSM and tau-PET signal survived FDR correction for multiple comparisons ($P < 0.05$). The colour scale represents the Pearson correlation coefficient. (**E**) Correlation between signed-QSM and tau-PET signal in the inferior temporal gyrus. The translucent area around the regression line represents the 95% CI for the regression estimate. (**F**) Chart representing the mediation analysis (each model includes age sex and cognitive group as covariates). c = direct association between tau-PET signal and cortical thickness [$\beta = -0.096$, $P < 0.001$, CI: –0.128 to –0.07]; c' = association between tau-PET signal and cortical thickness accounting for the effect of QSM [$\beta = -0.084$, $P < 0.001$, CI: –0.116 to –0.05]; c-c' = mediation effect of QSM [$\beta = -0.012$, $P < 0.01$, CI: –0.023 to 0, QSM mediate the 13% (β_{ratio}) of the effect of tau-PET signal on cortical thickness].

work, with a larger cohort, is warranted. Furthermore, we cannot exclude the possibility that other factors associated with older age might contribute to changes in QSM weakening the association between QSM and tau-PET signal.

In the present study, a subset of the analysis was focused on the ITG, which is a region known to be severely affected by tau pathology in Alzheimer's disease, and that can be reliably assessed with tau-PET (Johnson *et al.*, 2016). The voxel-wise analysis as well as the region of interest-based analysis showed a pattern of associations between QSM and tau-PET that are consistent with the stereotypical spread of Alzheimer's disease. However, it is important to point out that in some critical structures, such as the entorhinal cortex, the statistical association was weak (i.e. left entorhinal: $r = 0.13$, $P < 0.05$ uncorrected; right entorhinal: $r = 0.14$, $P < 0.05$ uncorrected). The spatial specificity of the results deserves future investigation because at the current state it is not possible to rule out that technical limitations of QSM might compromise the homogeneity of the signal across regions and then the ability to detect associations in smaller and grossly atrophic regions such as entorhinal cortex. Further study using a higher field scanner (e.g. 7 T, which provides higher sensitivity and higher signal-to-noise ratio) might clarify this point (van Bergen *et al.*, 2016).

QSM is a relatively new technique, and some considerations must be taken into account when interpreting these results. While QSM is a widely accepted surrogate for tissue iron content, QSM actually measures magnetic susceptibility, a fundamental electromagnetic property that can be driven by other metals including copper, manganese and aluminium, as well as myelin and calcium. That said, the concentrations of other metals in the human brain appear to be too low to exert an influence on the MRI signal over and above the effects of intrinsic local variations of iron content (Krebs *et al.*, 2014). Abnormal levels of myelination could also, in theory, modulate QSM but this is also unlikely in practice; the cortical QSM contrast appears to be largely driven by iron content (Fukunaga *et al.*, 2010), which, coupled with the positive QSM shift detected in this study, support a scenario of cortical iron deposition, a finding that has consistently been reported in post-mortem iron studies in Alzheimer's disease (Bulk *et al.*, 2018*a*; Ayton *et al.*, 2019). An additional limitation is the cross-sectional nature of the present study design; longitudinal studies are therefore warranted to elucidate the causal association between iron accumulation and tau aggregation. Future studies will also investigate the possible relationship between QSM and other potential causes of neurodegeneration in Alzheimer's disease (e.g. neuroinflammation).

In conclusion, the present study provided *in vivo* evidence of a relationship between iron accumulation (measured with QSM) and both insoluble tau aggregates (tau-PET) and neuronal loss (structural MRI). These results advance our understanding of the role of iron dysregulation in Alzheimer's disease pathophysiology, and prompt new avenues for both research and treatment development work.

Acknowledgements

We would like to thank Theodor Rumetshofer for his help with data management and visualization.

Funding

The work presented was supported by the European Research Council (grant no. 311292 to O.H.), the Swedish Research Council (grant no. 2016-00906 to O.H.), the Knut and Alice Wallenberg Foundation (grant no. 2017-0383), the Marianne and Marcus Wallenberg Foundation (grant no. 2015.0125 to O.H.) and the Swedish Alzheimer's Foundation (grant nos. AF-745911 to O.H., AF-838871 to N.S.).

Competing interests

O.H. has acquired research support (for the institution) from Roche and GE Healthcare. J.A-C. has equity and a full-time appointment at Tenoke Limited. The other authors report no competing interests.

Supplementary material

Supplementary material is available at *Brain* online.

References

Acosta-Cabronero J, Betts MJ, Cardenas-Blanco A, Yang S, Nestor PJ. In Vivo MRI mapping of brain iron deposition across the adult lifespan. J Neurosci 2016; 36: 364–74.

Acosta-Cabronero J, Cardenas-Blanco A, Betts MJ, Butryn M, Valdes-Herrera JP, Galazky I, et al. The whole-brain pattern of magnetic susceptibility perturbations in Parkinson' s disease. Brain 2017; 140: 118–31.

Acosta-Cabronero J, Machts J, Schreiber S, Abdulla S, Kollewe K, Petri S, et al. Quantitative susceptibility MRI to detect brain iron in amyotrophic lateral sclerosis. Radiology 2018a; 289: 195–203.

Acosta-Cabronero J, Milovic C, Tejos C, Callaghan MF. A robust multi-scale approach to quantitative susceptibility mapping. Neuroimage 2018b; 183: 7–24.

Acosta-Cabronero J, Williams GB, Cardenas-Blanco A, Arnold RJ, Lupson V, Nestor PJ. In vivo quantitative susceptibility mapping (QSM) in Alzheimer's disease. PLoS One 2013; 8: e81093.

Ayton S, Fazlollahi ÃA, Bourgeat P, Raniga P, Ng A, Lim YY, et al. Cerebral quantitative susceptibility mapping predicts amyloid-b-related cognitive decline. Brain 2017; 140: 2112–9.

Ayton S, Lei P. Nigral iron elevation is an invariable feature of parkinson's disease and is a sufficient cause of neurodegeneration. Biomed Res Int 2014; 2014: 1–9.

Ayton S, Wang Y, Diouf I, Schneider JA, Brockman J, Clare M, et al. Brain iron is associated with accelerated cognitive decline in people with Alzheimer pathology. Mol Psychiatry 2019.

Betts MJ, Acosta-Cabronero J, Cardenas-Blanco A, Nestor PJ, Düzel E. NeuroImage High-resolution characterisation of the aging brain using simultaneous quantitative susceptibility mapping (QSM) and R 2 * measurements at 7 T. Neuroimage 2016; 138: 43–63.

Blennow K, Hampel H, Weiner M, Zetterberg H. Cerebrospinal fluid and plasma biomarkers in Alzheimer disease. Nat Rev Neurol 2010; 6: 131–44.

Braak H, Braak E. Neuropathological stageing of Alzheimer-related changes. Acta Neuropathol 1991; 82: 239–59.

Bulk M, Abdelmoula WM, Nabuurs RJA, van der Graaf LM, Mulders CWH, Mulder AA, et al. Postmortem MRI and histology demonstrate differential iron accumulation and cortical myelin organization in early- and late-onset Alzheimer's disease. Neurobiol Aging 2018; 62: 231–42.

Bulk M, Kenkhuis B, Van Der Graaf LM, Goeman JJ, Natté R, Van Der Weerd L. Postmortem T2*-weighted MRI imaging of cortical iron reflects severity of Alzheimer's disease. J Alzheimer's Dis 2018; 65: 1125–37.

Cho H, Choi JY, Hwang MS, Kim YJ, Lee HM, Lee HS, et al. In vivo cortical spreading pattern of tau and amyloid in the Alzheimer disease spectrum. Ann Neurol 2016; 80: 247–58.

Dixon SJ, Lemberg KM, Lamprecht MR, Skouta R, Zaitsev EM, Gleason CE, et al. Ferroptosis: an iron-dependent form of nonapoptotic cell death. Cell 2012; 149: 1060–72.

Everett J, Céspedes E, Shelford LR, Exley C, Collingwood JF, Dobson J, et al. Evidence of redox-active iron formation following aggregation of ferrihydrite and the Alzheimer's disease peptide β-amyloid. Inorg Chem 2014; 53: 2803–9.

Fukunaga M, Li T-Q, van Gelderen P, de Zwart JA, Shmueli K, Yao B, et al. Layer-specific variation of iron content in cerebral cortex as a source of MRI contrast. Proc Natl Acad Sci U S A 2010; 107: 3834–9.

Griswold MA, Jakob PM, Heidemann RM, Nittka M, Jellus V, Wang J, et al. Generalized autocalibrating partially parallel acquisitions (GRAPPA). Magn Reson Med 2002; 47: 1202–10.

Hayes AF. Beyond Baron and Kenny: statistical Mediation Analysis in the New Millennium. Commun Monogr 2009; 76: 408–20.

Jack CR, Bennett DA, Blennow K, Carrillo MC, Dunn B, Haeberlein SB, et al. NIA-AA research framework: toward a biological definition of Alzheimer's disease. Alzheimer's Dement 2018; 14: 535–62.

Jack CR, Wiste HJ, Weigand SD, Therneau TM, Lowe VJ, Knopman DS, et al. Defining imaging biomarker cut points for brain aging and Alzheimer's disease. Alzheimer's Dement 2017; 13: 205–16.

Johnson KA, Schultz A, Betensky RA, Becker JA, Sepulcre J, Rentz D, et al. Tau PET imaging in aging and early Alzheimer's disease. Ann Neurol 2016; 79: 110–9.

Kim HG, Park S, Rhee HY, Lee KM, Ryu CW, Rhee SJ, et al. Quantitative susceptibility mapping to evaluate the early stage of Alzheimer's disease. NeuroImage Clin 2017; 16: 429–38.

Krebs N, Langkammer C, Goessler W, Ropele S, Fazekas F, Yen K, et al. Assessment of trace elements in human brain using inductively coupled plasma mass spectrometry. J Trace Elem Med Biol 2014; 28: 1–7.

Kuwabara H, Comley RA, Borroni E, Honer M, Kitmiller K, Roberts J, et al. Evaluation of 18 F-RO-948 PET for quantitative assessment of tau accumulation in the human brain. J Nucl Med 2018; 59: 1877–84.

Langkammer C, Schweser F, Krebs N, Deistung A, Goessler W, Scheurer E, et al. Quantitative susceptibility mapping (QSM) as a means to measure brain iron? A post mortem validation study. Neuroimage 2012; 62: 1593–9.

Lei P, Ayton S, Finkelstein DI, Spoerri L, Ciccotosto GD, Wright DK, et al. Tau deficiency induces parkinsonism with dementia by impairing APP-mediated iron export. Nat Med 2012; 18: 291–5.

Lovell MA, Xiong S, Xie C, Davies P, Markesbery WR. Induction of hyperphosphorylated tau in primary rat cortical neuron cultures mediated by oxidative stress and glycogen synthase kinase-3. J Alzheimer's. J Alzheimer's Dis 2004; 6: 659–71.

Maass A, Landau S, Horng A, Lockhart SN, Rabinovici GD, Jagust WJ, et al. Comparison of multiple tau-PET measures as biomarkers in aging and Alzheimer's disease. Neuroimage 2017; 157: 448–63.

Pérez M, Valpuesta JM, de Garcini EM, Quintana C, Arrasate M, López Carrascosa JL, et al. Ferritin is associated with the aberrant tau filaments present in progressive supranuclear palsy. Am J Pathol 1998; 152: 1531–9.

Rossor MN, Fox NC, Mummery CJ, Schott JM, Warren JD. The diagnosis of young-onset dementia. Lancet Neurol 2010; 9: 793–806.

Sayre LM, Perry G, Harris PLR, Liu Y, Schubert KA, Smith MA. In situ oxidative catalysis by neurofibrillary tangles and senile plaques in Alzheimer's disease: a central role for bound transition metals. J Neurochem 2000; 74: 270–9.

van Bergen JMG, Li X, Hua J, Schreiner SJ, Steininger SC, Quevenco FC, et al. Colocalization of cerebral iron with Amyloid beta in Mild Cognitive Impairment. Sci Rep 2016; 6: 9.

Vogel J, Iturria-Medina Y, Strandberg OT, Smith R, Evans AC, Hansson O, et al. Spread of pathological tau proteins through communicating neurons in human Alzheimer's disease. bioRxiv: 555821 2019.

Ward RJ, Zucca FA, Duyn JH, Crichton RR, Zecca L.The role of iron in brain ageing and neurodegenerative disorders. The Lancet Neurology 2014; 13: 1045–60.

Yamamoto A, Shin RW, Hasegawa K, Naiki H, Sato H, Yoshimasu F, et al. Iron (III) induces aggregation of hyperphosphorylated τ and its reduction to iron (II) reverses the aggregation: implications in the formation of neurofibrillary tangles of Alzheimer's disease. J Neurochem 2002; 82: 1137–47.